Full-Band Monte Carlo Analysis of Electron Transport in Arbitrarily Strained Silicon

G. Karlowatz, E. Ungersboeck, W. Wessner, and H. Kosina
Institute for Microelectronics, TU Wien, Gußhausstraße 27–29/E360, 1040 Wien, Austria
Phone: +43-1-58801/36026, Fax: +43-1-58801/36099, E-mail: karlowatz@iue.tuwien.ac.at

Abstract—Full-band Monte Carlo simulations of electron transport in bulk Silicon under several strain conditions are performed. The band structures of Si for arbitrary stress and strain conditions are calculated using the empirical non-local pseudopotential method. To restrict the EPM calculation to the smallest possible domain the symmetry properties for a given stress condition are taken into account. Results for biaxially strained Si grown on a [001] oriented $Si_{1-x}Ge_x$ substrate and for uniaxial tensile stress in [110] direction exhibit a high mobility enhancement. The effective masses and the energy splitting of the valleys extracted from the band structure explain the mobility gain observed in the simulation results. It is shown that the effective masses can change considerably under certain stress conditions.

I. INTRODUCTION

Over decades performance gains and increasing integration density of CMOS devices where successfully obtained by down-scaling. This process is getting more and more cost intensive as it is pushed closer to some principal physical limits. As an alternative strain engineering can be used to achieve higher device performance by increasing the carrier mobility in the desired semiconductor. Si basically shows two effects which contribute to this mobility gain, a reduction of the conductivity effective mass and reduced scattering. The latter is introduced mainly by the anisotropic shift of the Δ_6-valleys. Usage of strained Si for performance enhancement in CMOS devices started with a Si layer epitaxially grown on a relaxed SiGe substrate. The thin Si layer takes the larger lattice constant of the SiGe substrate and therefore gets biaxially tensile strained. Later a technique using capping layers was introduced to implement uniaxially stressed Si in CMOS devices. This technique overcomes a few technologically drawbacks of biaxially strained Si layers, related to problems of misfit and threading dislocations as well as diffusion. CMOS devices with uniaxially stressed channels in [110] direction are already fabricated in large volumes [1]. While biaxially strained Si has been studied in previous works [2][3], uniaxially strained Si is little investigated in terms of Monte Carlo simulation, although it is favored by the microelectronics industry as a key feature to enhance the 90, 65, and 45nm technology nodes [4]. In this work we use the VIENNA MONTE CARLO SIMULATOR (VMC) [5], which can handle arbitrarily strained Si. Results are shown for biaxially strained Si as well as for uniaxial tensile stress in [110] direction.

II. BAND STRUCTURE CALCULATION

For full-band Monte Carlo simulations a numerical representation of the band structure in the unit cell of the reciprocal lattice, the so-called *Brillouin zone*, is used to capture the dependence of the carrier energy on the wave vector. Because of symmetry only a part of the Brillouin zone – the *irreducible wedge* – has to be considered for band structure calculation. The volume of the irreducible wedge is determined by the number of symmetry elements $P(\Gamma)$ at the center of the Brillouin zone of the strained lattice via $\Omega_{\text{irred}} = \Omega_{\text{BZ}}/P(\Gamma)$. Strain and stress alters the band structure and reduces the crystal symmetry. For the diamond type lattice of relaxed Si $P(\Gamma) = 48$, for stress along [100], [111], and [110] $P(\Gamma)$ is equal to 16, 12, and 8, respectively, while for stress along some arbitrary direction the lattice is invariant to inversion only, thus $P(\Gamma) = 2$. Figure 1 shows the irreducible wedges for stress in [100], [111], and [110] direction.

The empirical non-local pseudopotential method (EPM) [6] is generalized to arbitrary stress/strain conditions to calculate the band structures of Si.

For discretization of the band-structure an unstructured tetrahedral mesh is used. Mesh refinement guarantees high resolution around the band minima, while a relatively low total number of mesh elements is maintained [7].

III. EFFECTIVE MASS CHANGE AND VALLEY SPLITTING

Experiments [8][9] have shown that the electron mobility enhancement in strained Si cannot solely be attributed to the energy splitting of the valleys. A recent study has shown that a stress along the [110] direction leads also to a change of the effective mass [10]. In Figure 2 the strain induced valley splitting is shown for biaxially strained and uniaxially stressed Si along [110] and [120] directions. It can be seen that biaxial tension is more effective in splitting the conduction band valleys than uniaxial tension. The in-plane effective masses of the lowest valley were extracted from EPM calculations. Figure 3 shows that uniaxial tensile stress along [110] yields the most pronounced Δm_{t}. This explains the pronounced anisotropy of the mobility in the transport plane as discussed in Section V. The change Δm_{t} is negligible for biaxial tensile strain. This result points out another advantage of uniaxially stressed Si over biaxially strained Si. For high uniaxial stress levels in [110] direction the mobility enhancement originates mostly from the reduced conductivity mass, which is almost linearly reduced with increasing stress. Therefore no mobility saturation occurs.
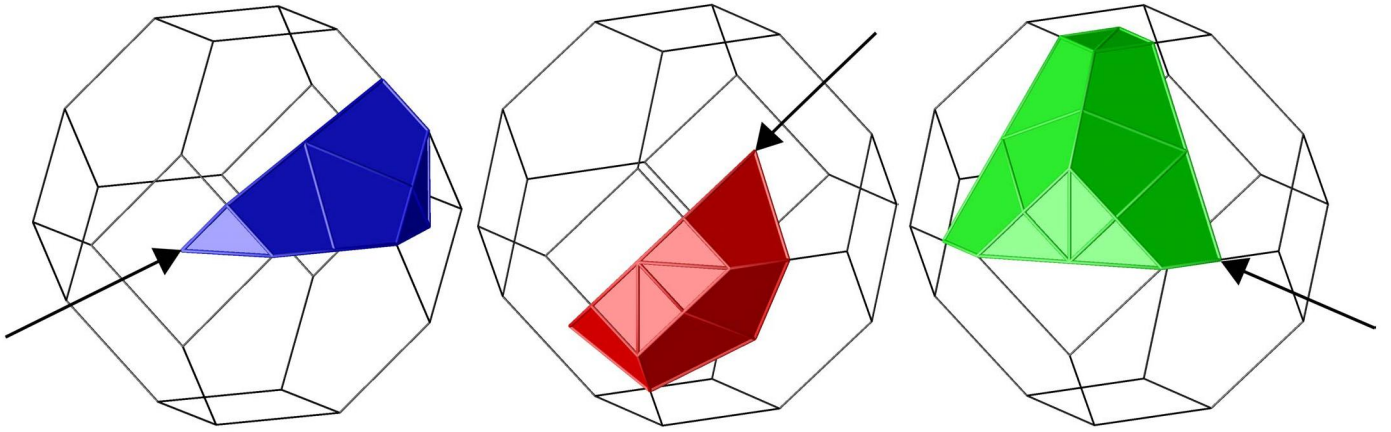
Figure 1: Irreducible wedges for stress applied in [100], [111], and [110] direction.

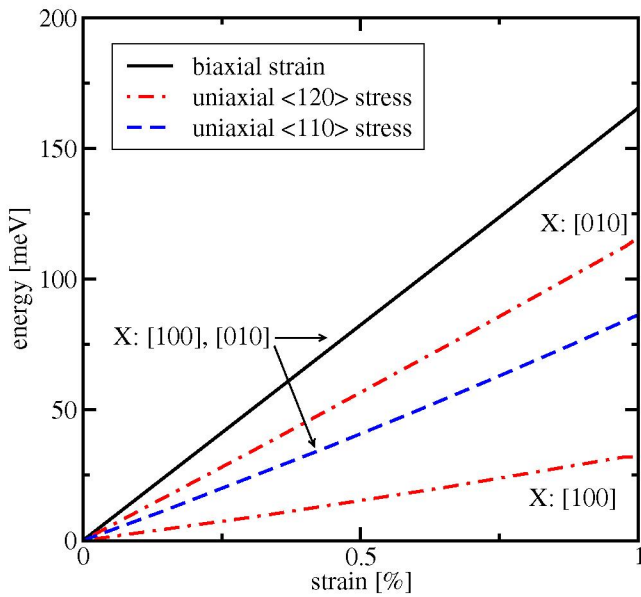**Figure 2:** Effect of biaxial tensile strain and uniaxial [110] and [120] tensile stress on valley splitting. The strain component in the stressed direction is shown.

Figure 3: Effect of biaxial tensile strain and uniaxial [110] and [120] tensile stress on the in-plane masses of the lowest valley.

IV. THE VIENNA MONTE CARLO SIMULATOR

VMC offers simulation algorithms for both bulk semiconductors and one-dimensional devices based on analytical and full-band models. Additionally, a fast zero-field algorithm for degenerate statistics is included [11]. VMC provides a comprehensive set of scattering models including phonon scattering, ionized impurity scattering, alloy scattering, and impact ionization. For full-band simulation phonon scattering models with constant matrix elements are used [12]. In this formulation the scattering rates are proportional to the density of final states, which is calculated from the band structure. The coupling constants Δ, the phonon energies and the phonon modes for inelastic optical and acoustic phonon scattering are given in Table I. The deformation potential for elastic intravalley acoustic phonons is assumed to be 8.5 eV. These parameters are used for relaxed and strained Si.
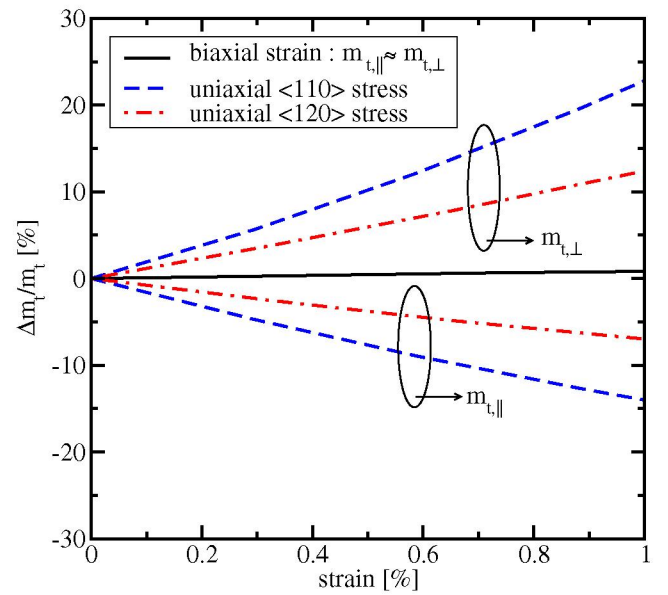
Impact ionization is modeled using a modified threshold expression [13]

$$S^{\mathrm{II}} = \begin{cases} P_1 \cdot \left(\epsilon - \epsilon_{\mathrm{th}}^1\right)^3 & : \epsilon_{\mathrm{g}} < \epsilon < \epsilon_{\mathrm{g}} + 622\mathrm{meV} \\ P_2 \cdot \left(\epsilon - \epsilon_{\mathrm{th}}^2\right)^2 & : \epsilon_{\mathrm{g}} + 622\mathrm{meV} < \epsilon \end{cases} \quad (1)$$

where S^{II} is the impact ionization scattering rate, ϵ is the electron energy, ϵ_{g} is the band gap energy, ϵ_{th}^1 and ϵ_{th}^2 are threshold energies, and P_1 and P_2 are multiplication factors which determine the softness of the threshold. The parameters are tuned to reproduce reported electron velocity field characteristics [14] and impact ionization coefficients [15][16][17] for relaxed Si: $\epsilon_{\mathrm{th}}^1 = \epsilon_{\mathrm{g}}$, $\epsilon_{\mathrm{th}}^2 = \epsilon_{\mathrm{g}} + 444\mathrm{meV}$, $P_1 = 4.5 \cdot 10^{11}\mathrm{s}^{-1}$ and $P_1 = 3.4 \cdot 10^{12}\mathrm{s}^{-1}$. For stressed/strained Si the threshold values are adjusted in accordance with the bandgap change.
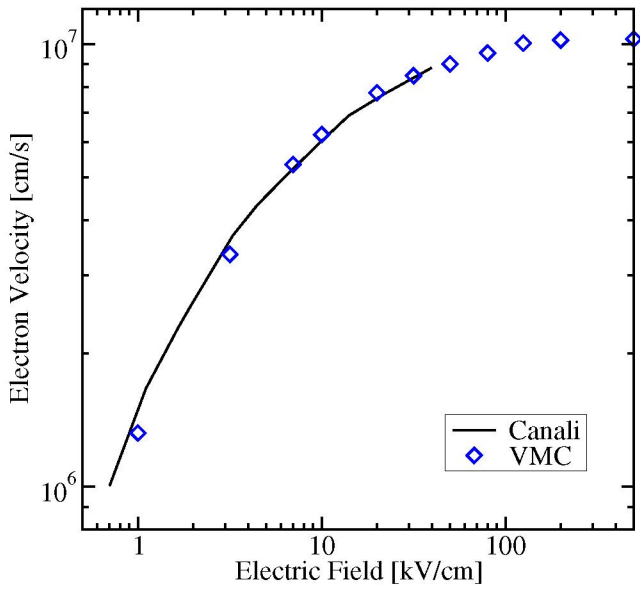
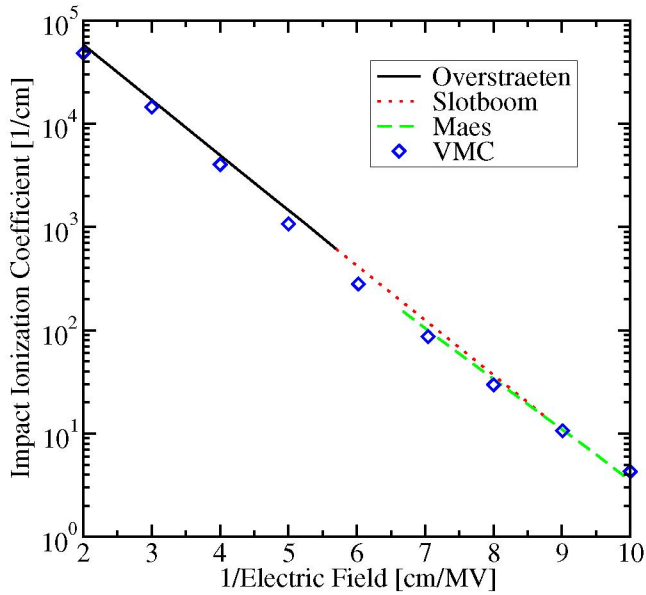**Figure 4:** Electron velocity versus field in [100] direction for relaxed Si compared to measurement [14].

Figure 5: Impact ionization coefficient versus inverse electric field compared to measurements [15][16][17].

Phonon Mode	Δ [MeV/cm]	$\hbar\omega$ [meV]
Transversal Acoustic f	47.2	12.1
Longitudinal Acoustic f	75.5	18.5
Longitudinal Optical f	1042	62.0
Transversal Acoustic g	34.8	19.0
Longitudinal Acoustic g	232	47.4
Transversal Optical g	232	58.6

TABLE I: Phonon Modes, coupling constants and phonon energies of inelastic phonon scattering.

Figure 4 shows the electron velocity as a function of the electric field in [100] direction for relaxed Si. Fig 5 shows the impact ionization coefficient over the inverse electric field. These results are compared to values from literature and show good agreement.

V. RESULTS

Figure 6 depicts the in-plane low field mobility versus Ge mole fraction of the $Si_x Ge_{1-x}$ substrate. Since the lattice constant of SiGe is larger than that of Si the resulting strain is tensile. For a mole fraction x = 0.4 the low field electron mobility is enhanced by a factor of 1.68 to 2410 cm^2/Vs. For Ge mole fractions above 0.2 a saturation can be observed. In biaxially tensile strained Si, two of the initially six-fold degenerated Δ_6-valleys are shifted down in energy and four are shifted up, which produces the band splitting shown in figure 2. With increasing strain the lower valleys are fully populated and the intervalley scattering to higher valleys is suppressed. From this point on the low field mobility does not benefit from further increasing the strain levels and mobility saturation occurs.

Figure 7 depicts the in-plane electron mobility at low electric field for uniaxial tensile stress. A strong anisotropy with the most pronounced mobility enhancement in stress direction can be observed. A stress level of 1.5GPa enhances the low field mobility by a factor of 1.63 to 2330 cm^2/Vs. Contrary to biaxial strain there is no saturation of the mobility enhancement. Note that compressive stress instead of tensile stress could also be used for electron mobility enhancement. The most pronounced enhancement is then achieved perpendicular to the applied stress in [$\bar{1}$10] direction, otherwise the result looks similar as in Figure 7.

Figure 8 presents the velocity field characteristics for uniaxial tensile stress in [110] direction and field in [110] and
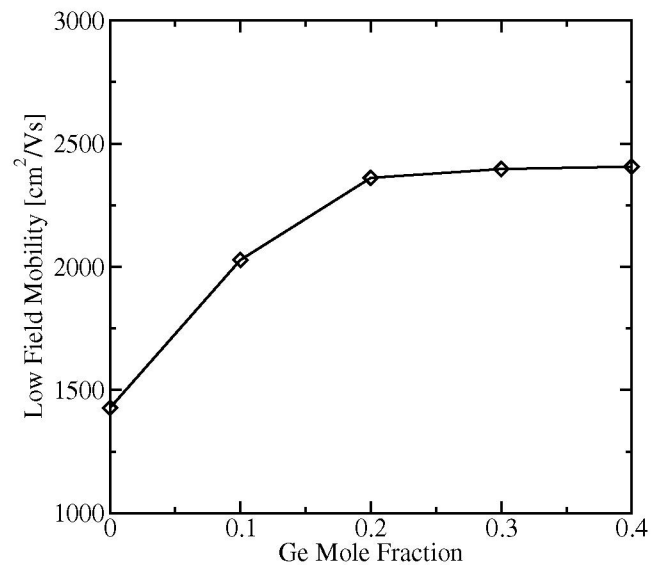

Figure 6: In-plane low field mobility of electrons in biaxially strained Si grown on a $Si_x Ge_{1-x}$ substrate.
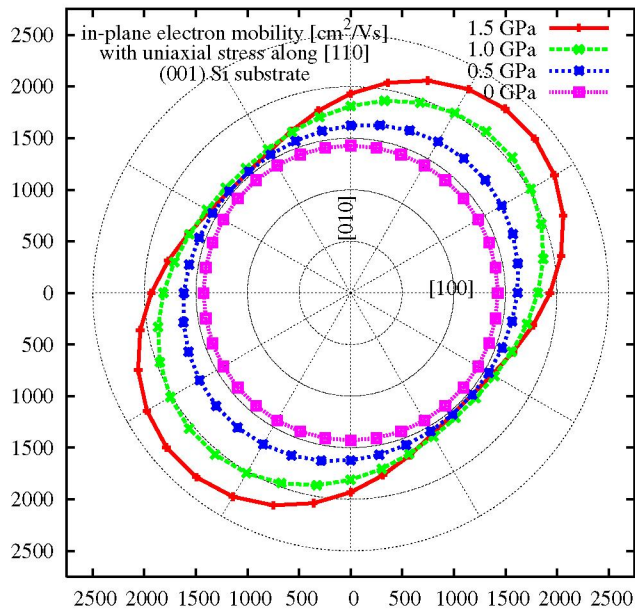
Figure 7: Low field electron mobility in bulk Si for uniaxial [110] tensile stress.
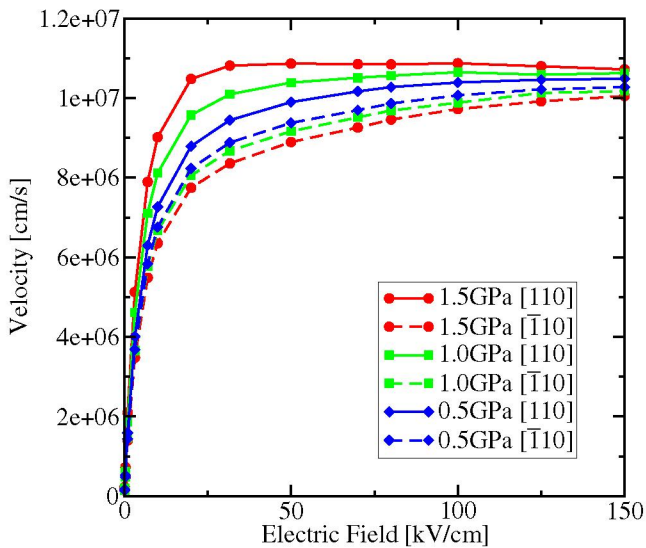

Figure 8: Electron velocity as a function of the electric field for field and stress in [110] direction.

the orthogonal [$\bar{1}$10] direction. As applied stress is rising, the curves for field in [110] direction show a steeper slope in the low field regime and exhibit a higher saturation velocity.

VI. CONCLUSION

A full-band Monte Carlo simulator which efficiently handles arbitrary stress and strain conditions is presented and used to analyze biaxially and uniaxially stressed Si. It is demonstrated that both biaxially strained Si grown on a SiGe substrate as well uniaxially stressed Si feature significantly enhanced electron mobility as compared to bulk Si. It can be concluded

that uniaxially stressed Si in [110] direction will be the preferred application because it exhibits no saturation of the low field mobility enhancement. Analysis of the band structure shows that this behavior can be explained by a large effective mass change for Si under uniaxial stress in [110] direction.

VII. ACKNOWLEDGMENT

REFERENCES

[1] T. Ghani, M. Armstrong, C. Auth, M. Bost, P. Charvat, T. Hoffmann, K. Johnson, C. Kenyon, J. Klaus, B. McIntyre, K. Mistry, J. Sandford, M. Silberstein, S. Sivakumar, P. Smith, K. Zawadzki, S. Thompson, and M. Bohr, IEDM Tech. Dig. 978 (2003).

[2] M. V. Fischetti and S. Laux, J. Appl. Phys. **80**, 2234 (1996).

[3] C. Jungemann and B. Meinerzhagen, *Hierarchical Device Simulation*, 1st ed. (Springer, Wien New York, 2003).

[4] S. E. Thompson, G. Sun, Y. S. Choi, and T. Nishida, IEEE Transaction on Electr. Devices **53**, 1010 (2006).

[5] T. Grasser, H. Kosina, and S. Selberherr, *VMC 2.0 User's Guide*, http://www.iue.tuwien.ac.at/software/vmc, Austria, 2006.

[6] M. Rieger and P. Vogl, **48**, 14276 (1993).

[7] G. Karlowatz, W. Wessner, and H. Kosina, Mathmod **1**, 316 (2006).

[8] H. Irie, K. Kita, K. Kyuno, and A. Toriumi, IEDM Techn. Dig. 225 (2004).

[9] K. Uchida, R. Zednik, C.-H. Lu, H. Jagannathan, J. McVittie, P. McIntyre, and Y. Nishi, IEDM Techn. Dig. 229 (2004).

[10] K. Uchida, T. Krishnamohan, K. Saraswat, and Y. Nishis, IEDM Techn. Dig. 129 (2005).

[11] S. Smirnov, H. Kosina, M. Nedjalkov, and S. Selberherr, *Lecture Notes in Computer Science*, 1st ed. (Springer, 2000 N.W. Corporate Blvd. ,Boca Raton, Florida 33431, 2003), pp. 185–193.

[12] C. Jacoboni and L. Reggiani, Rev. Mod. Phys. **55**, 645 (1983).

[13] E. Cartier, M. V. Fischetti, E. A. Eklund, and F. R. McFeely, Appl. Phys. Lett. **62**, 3339 (1993).

[14] C. Canali, C. Jacoboni, F. Nava, G. Ottaviani, and A. Alberigi-Quaranta, Phys. Rev. B **12**, 2265 (1975).

[15] J. Slotboom, G. Streutker, G. Davids, and P. Hartog, IEDM 494 (1987).

[16] W. Maes, K. D. Meyer, and R. V. Overstraeten, Solid State Electron. **33**, 705 (1990).

[17] R. van Overstraeten and H. de Man, Solid State Electron. **13**, 583 (1970).